

Operational assimilation of spectral wave data from the Sofar Spotter network

Isabel A. Houghton, Christie Hegermiller, Camille Teicheira, Pieter B. Smit

Sofar Ocean Technologies, San Francisco, CA

Key Points:

- A global network of over 600 drifting surface buoys reporting directional wave spectra every hour has been established.
- Assimilation of wave spectra yields quantifiable wave forecast improvements over traditional assimilation using significant wave height.
- Data from a new global ocean sensor and advances in wave data assimilation provide a direct path to improved marine weather forecasts.

Corresponding author: Isabel A. Houghton, isabel.houghton@sofarocean.com

Abstract

Historically, the sparseness of in situ open-ocean wave and weather observations has severely limited the forecast skill of weather over the ocean with major social and economic consequences for coastal communities and maritime industries. Ocean surface waves, specifically, are important for the interaction between atmosphere and ocean, and thus key in modeling weather and climate processes. Here, we investigate the improvements achievable from a large distributed sensor network combined with advances in assimilation strategies. Wave spectra from a global network of over 600 Sofar Spotter buoys are assimilated into an operational global wave forecast via optimal interpolation to update model spectra to best fit observations. We demonstrate end-to-end improvements in forecast skill of significant wave height of 38%, and up to 45% for other bulk parameters. This shows distributed observations of the air-sea interface, with advances in assimilation strategies, can reduce uncertainty in forecasts to dramatically improve earth system modeling.

Plain Language Summary

Historically, wave and weather observations are very sparse in the open ocean due to the cost and complexity of instruments and deployments. This lack of real-time weather information results in low-fidelity forecasts. Technological advances have led to the development of the Sofar sensor network, a distributed weather network spanning all the major oceans, consisting of over 600 free-drifting buoys that measure the ocean surface dynamics in great detail (including wave directional spectra). In this work we investigate how such large networks can be successfully used to meaningfully improve forecast accuracy using a new assimilation strategy to ingest the data into operational numerical forecast models. We show substantial improvements in forecast accuracy of the ocean wave field, which has broad implications for earth system modeling and will be directly relevant to coastal communities, marine renewable energy operations, and the efficiency of other maritime industries.

1 Introduction

The ability to observe and accurately predict the dynamics of the ocean interface is critically important for modeling air-sea exchanges, lower-atmosphere dynamics, safety at sea, and mitigation of coastal hazards due to extreme weather events. In general, the skill and accuracy of any weather forecast model fundamentally relies on the availability and successful assimilation of real-time data. In fact, data assimilation (DA) is widely deployed across all disciplines of operational numerical weather prediction and generally contributes as much to the skill of the forecast as the quality of the forecast model itself (Kalnay, 2002; Buizza et al., 2005). With the increase in available data and advances in assimilation strategies, the balance of performance skill will further shift toward data and advances in DA. This work explores how new, globally distributed sensing paradigms combined with advances in assimilation strategies can rapidly accelerate our ability to predict the future state of the air-sea interface.

Despite the importance of the air-sea interface for both ocean and lower-atmosphere dynamics, operational DA in wave models remains uncommon. This is in part due to a lack of suitable data, and in part due to the limitations of existing assimilation strategies that only adjust the total energy of the sea state, but not the distribution of energy. As a result, the benefits of assimilation into wave models is limited (Thomas, 1988; Lionello et al., 1992; Smit et al., 2021). By limiting the assimilation to bulk energy corrections only, traditional wave assimilation cannot address errors across different length scales (e.g. swell or sea components). Consequently, the assimilation improvements usually de-correlate on time scales of typical wind-wave coupling (i.e., under 24 hours) and there is limited value in adding more data to the DA. Fundamental to this, the wave problem is an arbitrary mix of an initial value problem (swell) and boundary value problem

(sea), with very different persistence time scales. For example, swell fields exhibit limited interaction with the atmosphere and DA error corrections can persist on the timescale of cross-basin propagation (2-3 weeks). In contrast, shorter waves (sea) are generally strongly coupled to local wind fields, which will dictate persistence of error corrections. To effectively assimilate into a spectral wave model and capture the range of persistence time scales, it is thus critical to correct errors in every component of the spectral distribution.

For such a wave DA strategy to be effective, observations of the wave spectrum are necessary. However, these data have historically been exceedingly sparse – satellite remote sensing is generally limited to bulk parameters (e.g. total energy) and in-situ observations were previously not available in the open ocean. Recently, through advances in mobile technology, satellite communication networks, and improvements in photovoltaic and battery technology, new compact sensor platforms have become available that can deliver scalable, in situ, long-dwell wave spectrum observations. To date, the largest of such wave observing system is the Sofar Spotter network, which is composed of over 600 globally distributed, free-drifting marine weather buoys. (Raghukumar et al., 2019; Voermans et al., 2020; Houghton et al., 2021). This distributed sensor network opens up the opportunity to develop the first operational spectral wave-DA.

Given the historical rarity of buoy spectral information at scale, effective methods to assimilate those data remain uncommon and, to date, have not been widely operationalized. A specific challenge, addressed in the work here, is buoy spectral information is only available as the one-dimensional frequency spectrum and first four directional Fourier components, rather than the two-dimensional frequency-directional (or wavenumber) spectrum that is the model state (Kuik et al., 1988). Thus, an assimilation strategy that relates the observations to the model state is necessary.

Previously, a few studies have explored optimal interpolation based methods for spectra-based assimilation using pitch-and-roll buoy data in a narrow geographic region (Hasselmann et al., 1997; Voorrips et al., 1997). In that method, the analysis was conducted by dividing the spectrum into discrete partitions and updating the model state based on the bulk statistics of each observed partition, substantially reducing the variables describing the wave spectrum. The complexity was then primarily the partitioning of the spectrum and the cross-assignment of partitions between model and observations, which was accomplished with heuristic methods despite possible ambiguities.

Here we present, in tandem, the establishment of a global distributed sensor network and an efficient method for assimilating the observations provided into an operational wave forecast system. This work aims to evaluate the improved forecasting ability made possible by the notable increase in available data, both in terms of geographic coverage and spectral detail. The two step spectra-based DA method outlined here is straightforward to implement and avoids ambiguity with cross-assignment between model and observations. Section 2 describes the buoy network, wave model, and assimilation framework. Results from a month-long reanalysis are presented in Section 3. Finally, impacts and conclusions are described in Section 4.

2 Methods

The DA strategy is built upon the previously established optimal interpolation framework described by Smit et al. (2021), where the initial wave field was updated via sequential optimal interpolation of the observed significant wave height with scaling of the two-dimensional wave action density spectrum to match the analysis wave heights at all grid points. However, this approach has well-documented limitations (Lionello et al., 1992; Portilla-Yandún & Cavaleri, 2016). Specifically, by scaling the spectrum solely by a constant factor derived from the ratio of the analysis wave height to background wave height, model errors in period and direction were left uncorrected. Also, distinct contributions

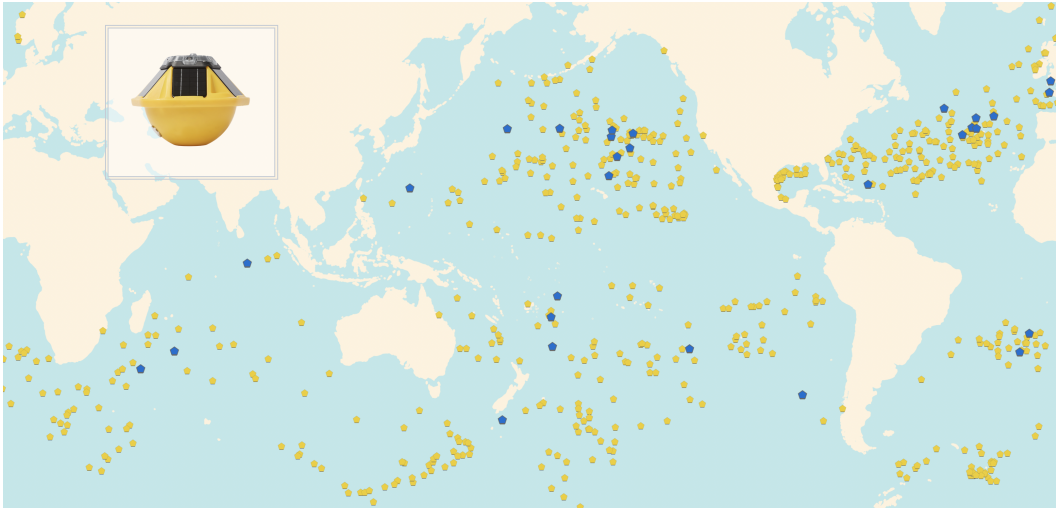


Figure 1. The global Sofar Spotter network (yellow pentagons). Twenty-nine buoys (blue) were randomly selected from the full network to be excluded from the analysis step to provide independent observations to compare with the nowcasts and forecasts. Inset: The 42 cm diameter Spotter buoy represented by pentagonal icons on the map.

112 to the wave field, e.g. a swell component, could be incorrectly modified despite achiev-
 113 ing parity with the bulk significant wave height at that location. While this method was
 114 found to produce improvements in both model nowcasts and forecasts, substantially more
 115 information is available from the Spotter buoys beyond significant wave height, specif-
 116 ically the variance density spectrum and the four Fourier coefficients. To fully utilize these
 117 observational data to update the initial state of the operational forecast model, the op-
 118 timal interpolation framework is augmented here to update the wave Fourier coefficients
 119 on a per-frequency basis and subsequently reconstruct the two-dimensional model spec-
 120 tra.

121 2.1 Spectral Buoy Data

122 The wave spectra observations are provided by a global network of free-drifting Spot-
 123 ter buoys developed by Sofar Ocean (Figure 1). The Spotter buoy is lightweight and com-
 124 pact (5.4 kg, 42 cm-diameter approximate sphere) and reports the variance density spec-
 125 trum and Fourier coefficients along with sea surface temperature, surface drift, baromet-
 126 ric pressure, inferred wind and sound level in near-real time (see Raghukumar et al. (2019);
 127 Houghton et al. (2021) for further buoy description and validation). The free-drifting buoys
 128 provide observations from a network that evolves continuously due to the underlying global
 129 currents. Nearly three years of network growth have indicated the sustaining ability to
 130 collect long-dwell observations with reliable spatial coverage.

131 The global Sofar Spotter network surpassed 600 buoys globally in March 2022 and
 132 is continuously expanding. The data is stored in a database with a modern API to fa-
 133 cilitate operational incorporation of buoy observations at an hourly cadence. As of De-
 134 cember 2020, all buoys in the network transmitted spectral data at frequencies from 0.293
 135 Hz to 0.8 Hz, with select buoys transmitting up to 1.25 Hz. The Spotter frequency grid
 136 is irregular, with higher resolution bins (0.0098 Hz bins) at frequencies below 0.3 Hz and
 137 lower resolution (0.029 Hz bins) at higher frequencies. The frequency dependent vari-
 138 ance density spectrum, e^{obs} , and four Fourier coefficients, a_1^{obs} , b_1^{obs} , a_2^{obs} , b_2^{obs} (with $^{\text{obs}}$
 139 denoting observation), at each Spotter location were calculated at thirty minute inter-

140 vals and reported hourly (i.e. two observations per transmission). Derived wave param-
 141 eters such as wave height, mean period, and direction are calculated according to stan-
 142 dard oceanographic practice ((Kuik et al., 1988)). In order to assimilate the Spotter buoy
 143 spectra, the data were interpolated onto the irregular wave model spectral grid (described
 144 below) using linear interpolation.

145 2.2 Wave Forecast Model

146 The WAVEWATCH3 model (WW3; Tolman et al. (2019)) is implemented over the
 147 global ocean at 0.5 degree horizontal resolution and forced by near-surface winds from
 148 the European Centre for Medium-Range Weather Forecasts (ECMWF) Integrated Fore-
 149 cast System (IFS) High Resolution (HRES) atmospheric and sea ice forecast. The model
 150 spectral space is discretized by 36 directions and 36 frequencies. Frequencies are loga-
 151 rithmically distributed with a growth factor of 1.1 from $f_1 = 0.035$ Hz to $f_3 = 0.98$ Hz
 152 (see) for full model configuration details). Atmospheric forcing is updated every six hours,
 153 at which time a 4- or 10-day operational forecast is initialized from the corresponding
 154 analysis for that hour.

155 The DA uses an hourly analysis cycle. This includes a one-hour WW3 forecast and
 156 an instantaneous analysis at the end of each hour to initialize the next forecast. The spectra-
 157 based DA method can be summarized as a two step process where (1) the variance den-
 158 sity and Fourier coefficients are optimally interpolated for every frequency bin to pro-
 159 duce analysis moments and (2) an analysis directional distribution is generated from a
 160 cost minimization targeted to match analysis moments and the model background di-
 161 rectional distribution. Details of these steps follow.

162 2.3 Optimal interpolation of Fourier coefficients

We define a reduced background state vector for DA as the variance density and
 Fourier coefficients at each frequency ($e^{\text{bg}}, a_1^{\text{bg}}, b_1^{\text{bg}}, a_2^{\text{bg}}, b_2^{\text{bg}}$, with ^{bg} denoting background).
 These may be obtained from the full model background state at analysis time through
 discrete approximations of the Fourier integrals of the directional distribution. Enumer-
 ating the N equidistant (resolution $\Delta\theta$) model directions as $\boldsymbol{\theta}^T = [\theta_1, \dots, \theta_N]$, the dis-
 cretely sampled directional distribution D_j is defined as $D_j^{\text{bg}}(f; \mathbf{x}) = E_j^{\text{bg}}/e^{\text{bg}}$, $E_j^{\text{bg}} =$
 $E(f, \theta_j; \mathbf{x})$ and

$$e^{\text{bg}}(f; \mathbf{x}) = \Delta\theta \sum_{\boldsymbol{\theta}} E^{\text{bg}}(f, \boldsymbol{\theta}; \mathbf{x}).$$

The Fourier coefficients, \mathbf{m} , of the directional distribution then follow as

$$\mathbf{m}^{\text{bg}}(f; \mathbf{x}) = \begin{bmatrix} (2\pi)^{-1} \\ a_1^{\text{bg}}(f; \mathbf{x}) \\ b_1^{\text{bg}}(f; \mathbf{x}) \\ a_2^{\text{bg}}(f; \mathbf{x}) \\ b_2^{\text{bg}}(f; \mathbf{x}) \end{bmatrix} = \Delta\theta \begin{bmatrix} (2\pi)^{-1} \mathbf{1}^T \\ \cos(\boldsymbol{\theta}^T) \\ \sin(\boldsymbol{\theta}^T) \\ \cos(2\boldsymbol{\theta}^T) \\ \sin(2\boldsymbol{\theta}^T) \end{bmatrix} \mathbf{D}^{\text{bg}}(f, \mathbf{x}) = \mathbf{M} \mathbf{D}^{\text{bg}}(f, \mathbf{x}) \quad (1)$$

163 with $\mathbf{D}^T = [D_1, \dots, D_N]$, $\mathbf{1}^T = [1, \dots, 1_N]$ and \mathbf{M} representing the discrete approxi-
 164 mation of the Fourier integration. The zeroth coefficient is known a-priori and describes
 165 the integration to one of the directional distribution in theta.

The analysis Fourier coefficients \mathbf{m}^{an} (^{an} denoting analysis) and analysis variance
 density e^{an} are obtained through optimal interpolation from the analysis equation which
 – following Smit et al. (2021) – is expressed as

$$\mathbf{y}^{\text{an}} = \mathbf{y}^{\text{bg}} + \underbrace{\boldsymbol{\rho} \mathbf{H}^T (\mathbf{H} \boldsymbol{\rho} \mathbf{H}^T + \sigma \mathbf{I})^{-1}}_{\mathbf{K}} (\mathbf{H} \mathbf{y}^{\text{bg}} - \mathbf{y}^{\text{obs}}) \quad (2)$$

166 Here $\mathbf{y}(f)$ (analysis or background) is the state vector of the model with M grid points
 167 for a given frequency, and $\mathbf{y}^{\text{obs}} = [y_j^{\text{obs}}(f), \dots, y_j^{\text{obs}}(f)]^T$ denotes the J observations of
 168 the state. Further, \mathbf{H} is a $J \times M$ bi-linear interpolation matrix that projects model es-
 169 timates to observed locations. Lastly, \mathbf{K} is the $M \times J$ Kalman Gain matrix that is de-
 170 pendent upon model error correlation, $\boldsymbol{\rho}$, and relative observation errors $\sigma \mathbf{I}$. Here, \mathbf{I} is
 171 the identity matrix and σ (set to 0.3 here, see Smit et al. (2021)) represents the obser-
 172 vational error scaled with a representative model error. Equivalent equations to (2) are
 173 used for the Fourier coefficients $a_1^{\text{an}}, b_1^{\text{an}}$, etc.

174 Optimal interpolation requires a-priori specification of the error-covariances (cor-
 175 relations here), which in general are non-trivial to determine. Here, we take ρ to be isotropic,
 176 stationary, homogeneous and independent of frequency, and use a parameterized form
 177 as in Smit et al. (2021) that de-correlates over a characteristic distance of 300 km. Fur-
 178 ther, inter-coefficient errors are assumed to be uncorrelated, allowing for independent
 179 application of (2) to individual moments.

180 2.4 Directional Reconstruction

The OI step performs DA in observational space. To return to model space, a sub-
 sequent step is needed to reconstruct the two-dimensional directional spectra at each model
 grid point to serve as the initial condition for the forecast. However, the analysis Fourier
 coefficients, \mathbf{m}^{an} , do not uniquely determine the analysis directional distribution because
 \mathbf{M} is under-determined and not invertible. To uniquely specify the directional distribu-
 tion, we assume that the model background distribution estimation, D^{bg} , is in general
 skillful, and seek a distribution that minimizes the difference with the model background
 under the constraints that D^{an} reproduces the analysis Fourier coefficients and is pos-
 itive semi-definite. Considering a single frequency at a single location \mathbf{x} , the analysis di-
 rectional distribution is the solution of the quadratic-programming problem,

$$\begin{aligned} \min_{D^{\text{an}}} & [D^{\text{an}} - D^{\text{bg}}]^T [D^{\text{an}} - D^{\text{bg}}] \\ \text{subject to} & \quad \mathbf{M}D^{\text{an}} = \mathbf{m}^{\text{an}} \\ & \quad D^{\text{an}} \geq 0 \end{aligned} \quad (3)$$

181 In practice, the reproduction of the Fourier coefficients is applied as a cost in addition
 182 to the difference from the background directional distribution and a least-squares bounded
 183 minimization is used. Following Equation 3, an analysis directional distribution is gen-
 184 erated for every model grid point. To return to the two-dimensional spectrum, the di-
 185 rectional distribution is then multiplied by $e^{\text{an}}(f)$, provided explicitly from the optimal
 186 interpolation step.

187 The optimization approach with constraints, inspired by (Crosby et al., 2017), is
 188 chosen over other methods, such as maximum entropy estimation (Lygre & Krogstad,
 189 1986), as it allows for the inclusion of the additional information provided by the model
 190 background. This assumes that although the model may be incorrect, it provides a rea-
 191 sonable starting point to generate the analysis distribution and further encourages spa-
 192 tial coherence across the geographic domain despite each grid point being updated in-
 193 dependently. Further, this formulation is sufficiently computationally efficient to remain
 194 within operational time constraints.

195 2.5 Reforecast Experiment

196 The spectra-based data assimilation scheme is evaluated with an approximately 32
 197 day reforecast experiment starting February 20th, 2022 and ending March 24, 2022. Three
 198 experiments are run in order to assess the impact of the DA methods: a free-running forced
 199 WW3 model forecast, an hourly-cycled DA case assimilating significant wave height ob-
 200 servations (henceforth H_s -based), and an hourly-cycled DA case assimilating wave spec-
 201 tra observations as described above (henceforth spectra-based). For each experiment, a

202 4-day forecast is initialized every 12 hours from the analysis state (or forecast state in
 203 the case of the free-running model). Twenty-nine Spotter buoys are excluded from the
 204 DA experiments for evaluation. To ensure global coverage of excluded buoys, all buoys
 205 are first binned into ten regions by latitude and longitude, and a random selection of 10%
 206 in that bin were chosen to be excluded (see Figure 1). In addition to the bulk param-
 207 eters output hourly over the entire model domain, two-dimensional model spectra are
 208 output hourly at the excluded Spotter locations (with buoy drift neglected over forecast
 209 timescales).

210 Forecast skill is evaluated by point-wise comparison of modeled variables to the Spot-
 211 ter observations. Spotter observations are linearly interpolated to the nearest hour and
 212 the modeled fields are bilinearly interpolated to the Spotter latitude and longitude.

213 To assess model skill in different frequency ranges, specifically low frequency swell
 214 energy versus high frequency wind sea energy, the observed and modeled variance den-
 215 sity spectra ($e(f)$) are partitioned at 0.08789 Hz. Only observations for which the Spot-
 216 ters reported the presence of swell are used to calculate the corresponding root-mean-
 217 square error of these partitioned sea states. Following methods from Portilla et al. (2009)
 218 for partitioning one-dimensional spectra, an estimate of the ratio between the peak en-
 219 ergy of the wave system and the peak energy of a Pierson–Moskowitz spectrum with the
 220 same peak frequency, γ^* , is calculated as an indicator of swell presence. Observations
 221 with a $\gamma^* < 0.5$ are used to select the observations for assessment of swell forecast skill
 222 (see Supplement for further details).

223 3 Results

224 3.1 Spectral Updates

225 The optimal interpolation step updates the frequency-binned moments to balance
 226 between the model background and observations. In general, this does not exactly match-
 227 ing either owing to the uncertainty prescribed to both the observations and forecasts in
 228 the relative standard deviation of the errors.

229 Spotter-0890 (Figure 2a), which was excluded from the DA experiments, illustrates
 230 the impact of the assimilation of each observation type. For the spectra in Figure 2b,
 231 the observed and non-assimilated modeled variance density spectra are different. For the
 232 H_s -based assimilation, the distribution is altered with higher energy at the peak frequency
 233 and lower energy at the higher frequencies, still different from the Spotter observation.
 234 The variance density spectrum for the spectra-based assimilation (blue line), however,
 235 closely matches the Spotter observation of the peak frequency as well as the distribu-
 236 tion of energy across frequencies, particularly capturing the wind-sea peak at higher fre-
 237 quencies. Further, the H_s -based assimilation does little to improve agreement of the Fourier
 238 coefficients with the Spotter observations (Figure 2c-f) while the spectra-based assim-
 239 ilation results in a notable qualitative improvement in agreement. Finally, the two-dimensional
 240 spectra from the non-assimilated model (g), spectra-based assimilated model (h), and
 241 their difference (i) illustrates the impact of assimilation of spectral information from a
 242 network of buoys. Specifically, energy was modified in both direction and frequency space
 243 – decreasing the energy and shifting to slightly lower frequencies around 300° , remov-
 244 ing a swell field around 100° , and introducing a swell field around 200° .

245 3.2 Improvements to Bulk Statistics

246 Direct validation of the analysis two-dimensional spectra, such as shown in Figure
 247 2h, remains challenging because directional wave buoys, like the Spotter, only provide
 248 the Fourier coefficients. However, an improved two-dimensional spectrum in the model

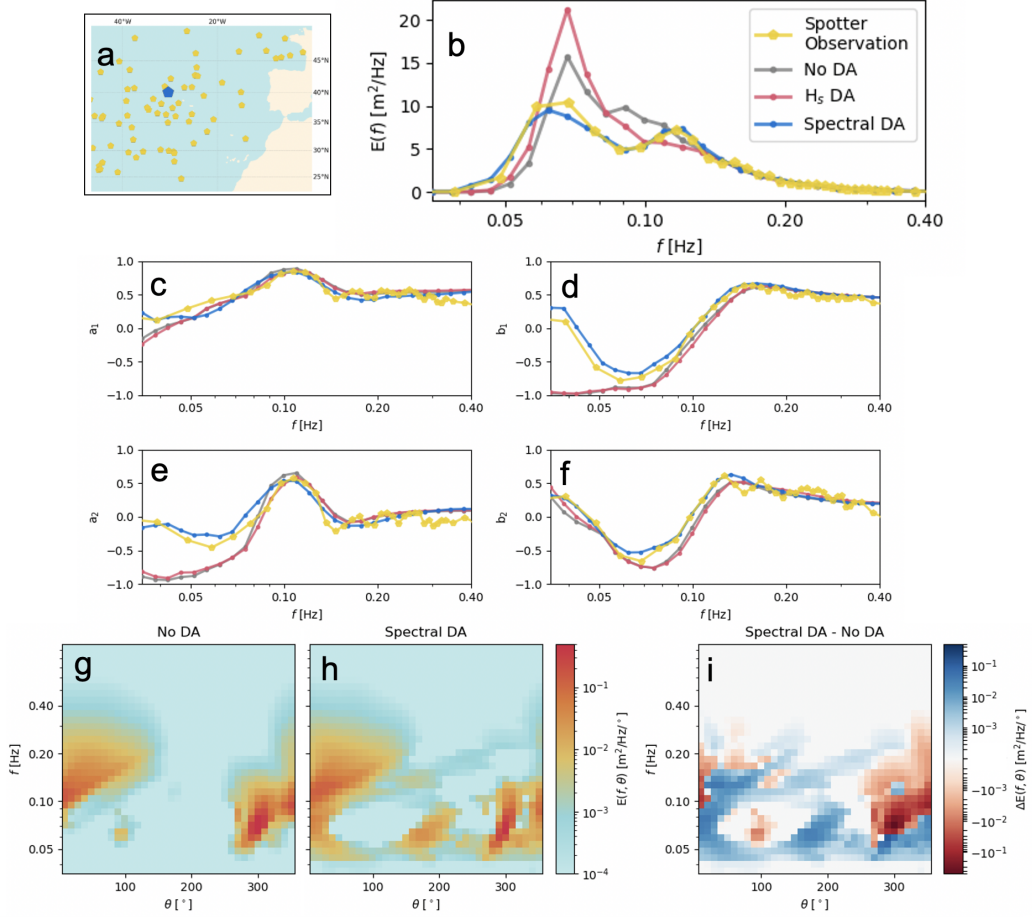


Figure 2. Model states from the different WW3 experiments at an excluded Spotter buoy (SPOT-0980) on Friday, March 4, 2022 12:00 UTC. (a) The location of the Spotter in the North Atlantic. (b) The variance density spectrum and (c-f) Fourier coefficients of the Spotter (yellow), free-running WW3 forecast (grey), wave height-assimilated (pink) and spectra-assimilated (blue). Moments are calculated from the WW3 model spectra. (g-h) The two-dimensional wave spectrum from the free-running WW3 forecast and spectra-assimilated DA case. (i) The difference between the two spectra.

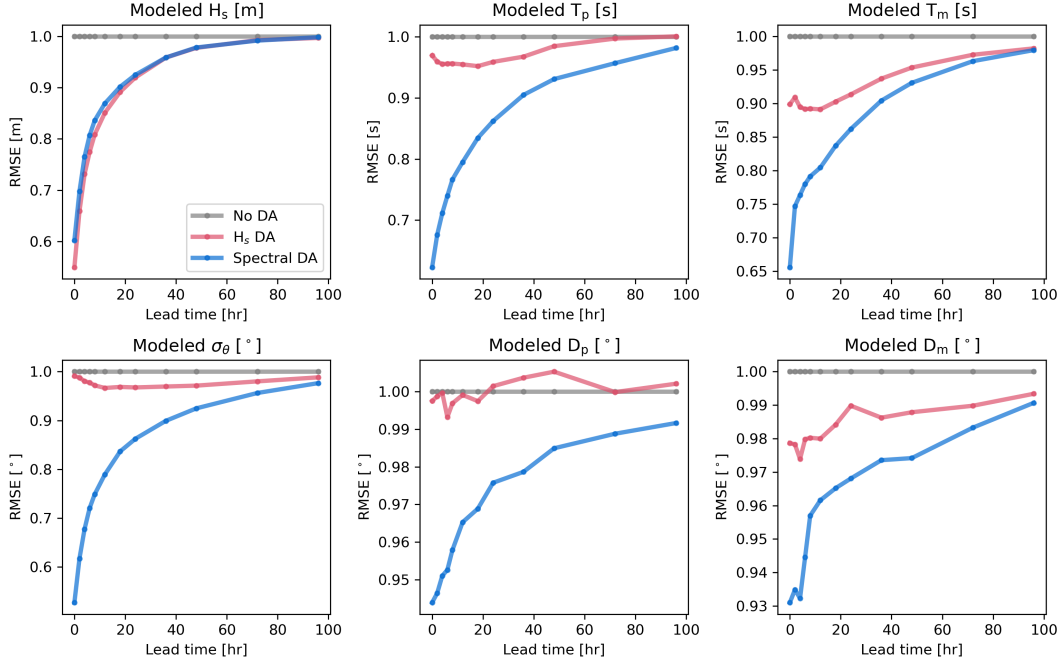


Figure 3. Root-mean-square error (RMSE) of bulk wave parameters in the analyses and forecasts up to four days from all three WW3 experiments. No assimilation (grey), H_s -based assimilation (pink), and spectra-based assimilation (blue) were assessed at all Spotter locations. Approximately 25,000 observation-model pairs were used to estimate the RMSE.

249 will propagate forward in time and space and manifest in the bulk parameters of the down-
 250 stream wave field.

251 Substantial improvements are observed in forecast skill when evaluated against Spot-
 252 ter bulk parameter observations (Figure 3). Significant wave height error in the anal-
 253 ysis is reduced by approximately 44% by the H_s -based assimilation approach and 38%
 254 by the spectra-based approach. At 24-hour lead times, the error is reduced by 8.2% and
 255 7.5% for H_s -based and spectra-based, respectively. At even longer lead times, the error
 256 reductions decay asymptotically to zero, with negligible forecast skill improvement be-
 257 yond 4 days.

258 Five other bulk parameters – peak period T_p , mean period T_m , directional width
 259 σ_θ , peak direction D_p , and mean direction D_m – consistently exhibited the largest er-
 260 ror reductions in the spectra-based DA case, with up to 45% reduction in errors for di-
 261 rectional width in the analyses and persistent reductions of 1-2% in 4-day forecasts across
 262 bulk parameters.

263 The full advantage of the spectra-based approach is illustrated in the bulk param-
 264 eters describing period and direction. The H_s -based approach does lead to some improve-
 265 ments in these bulk parameters despite no direct incorporation of this information into
 266 the assimilation scheme. Specifically, the H_s -based approach scales the energy spectrum
 267 equivalently across all frequencies, therefore not initially impacting the peak direction
 268 or frequency. However, as different portions of the wave spectrum relax to the forcing
 269 field (wind) at different rates (the higher frequencies adjusting the most rapidly), the scal-
 270 ing of the energy spectrum and subsequent relaxation to the background forcing will ul-
 271 timately modify the shape of the energy spectrum, in turn impacting the period and di-
 272 rection properties of the wave field. This evolution of the spectra results in the interme-

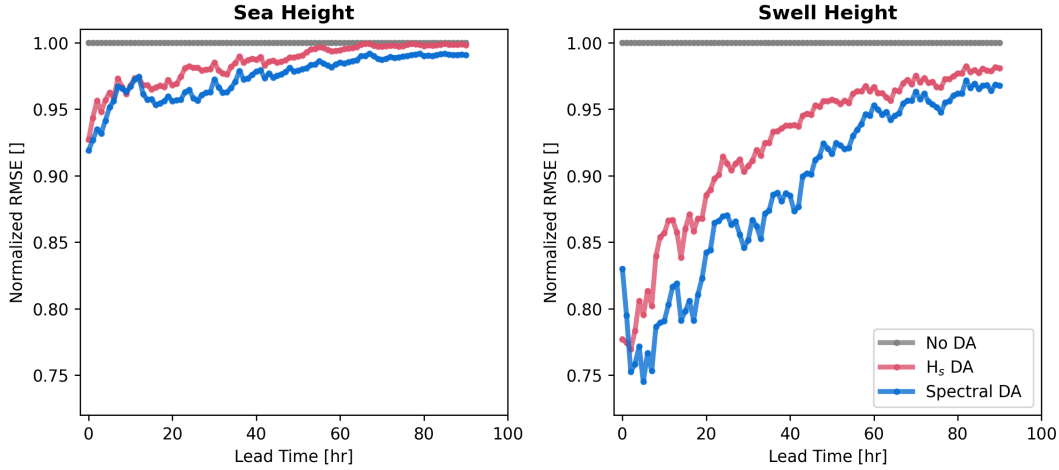


Figure 4. Wind sea significant wave height (left) and swell significant wave height (right) root-mean-square error normalized against the non-assimilated error (grey) for the H_s -based assimilation (pink) and spectra-based assimilation (blue) for observations with swell energy present (see supplement for further details).

273 diate improvements to the frequency and direction properties following the H_s -based ap-
 274 proach. The spectra-based approach, on the other hand, explicitly updates the spectrum
 275 to better match the Fourier coefficients, manifesting in marked improvements to all bulk
 276 parameters. In particular, the improvements to the bulk parameters extend to longer lead
 277 times, indicating the value of correcting the frequency and direction information to sub-
 278 sequently propagate across the geographic domain. While most modeling efforts are eval-
 279 uated in terms of significant wave height (likely because this is the primary open ocean
 280 data available), other parameters of the wave field are equally important to accurately
 281 represent (e.g., large container vessels can be extremely vulnerable to specific frequency
 282 waves even at low magnitudes, swell can steer wind stress, and short waves impact air-
 283 sea fluxes).

284 The approximately equivalent performance of the two assimilation strategies (H_s -
 285 based and spectra-based) when evaluated on just significant wave height is likely a re-
 286 sult of the spectra-based approach having additional constraints beyond the significant
 287 wave height target. Competing costs in reconstructing the directional distribution would
 288 then lead to less direct matching of the bulk parameter of significant wave height, de-
 289 spite better agreement with the spectral shape, with the largest impact at the zero-hour
 290 lead time.

291 While the bulk statistic of total significant wave height is most effectively addressed
 292 by H_s -based assimilation (Figure 3), when we consider the significant wave height of wind
 293 sea (higher frequency) versus swell (lower frequency), a differentiation of the effective-
 294 ness of the two assimilation methods becomes clear (Figure 4). Because the wind seas
 295 are tightly coupled to the surface winds, any modifications to the initial condition of the
 296 high frequency wave field rapidly relax to the wind forcing. However, the propagation
 297 of low frequency swell waves is, to the first-order, an initial value problem, and there-
 298 fore ideally suited to improvement via DA. By updating the wave fields with spectra-
 299 based assimilation, the initial state of the swell is better represented and more accurately
 300 propagated forward in time. The error of specifically swell-containing events was reduced
 301 up to 25% in the analysis, with persistent improvement of approximately 5% out to four
 302 days (Figure 4).

303 4 Discussion and Conclusions

304 Accurately predicting marine weather is critical to industry, society and the envi-
305 ronment – from reducing global shipping emissions and safety risks, to mitigating coastal
306 hazards. Observations and their effective utilization in numerical models play an out-
307 size role in progressing forecasting ability and, for the first time, in situ observations of
308 directional wave spectra are available in the open ocean at a sufficient density for im-
309 pact at global scales. The operational assimilation scheme described here specifically il-
310 lustrates the capacity for wave spectral observations to improve forecast accuracy of bulk
311 parameters and spectral characteristics. The incorporation of the wave spectral data in
312 the operational assimilation scheme quantitatively improves the forecast skill of signif-
313 icant wave height up to 38% over the free-running WW3 model, and was further shown
314 to outperform the H_s -based DA in forecasting period and direction, with particular suc-
315 cess for swell-dominated fields.

316 This work focuses on demonstrating the impact of distributed spectral observations
317 on wave forecast skill, but the potential for improvements is not limited to waves alone.
318 All interactions between oceans and the atmosphere are influenced by the ocean surface
319 (Cavaleri et al., 2012), with exchange processes typically strongly dependent on the spec-
320 tral distribution of energy. Consequently, through coupled data assimilation, a path ex-
321 ists to use spectral observations to improve exchanges between ocean and atmosphere,
322 thus improving earth system modeling more broadly. Overall, this work describes the
323 realization of observational networks to provide the needed data with proven accuracy
324 and reliability for such advances in operational models and lays the groundwork for broad
325 progress in coupled earth systems modeling.

326 **Acknowledgments**

327 Historical data from Spotter buoys, including those used in this study, is freely available
328 for research use by contacting Sofar Ocean Technologies (www.sofaroccean.com).

329 All data used in this analysis will be made openly available.

References

330

- 331 Buizza, R., Houtekamer, P. L., Toth, Z., Pellerin, G., Wei, M., & Zhu, Y. (2005,
332 5). A Comparison of the ECMWF, MSC, and NCEP Global Ensemble
333 Prediction Systems. *Monthly Weather Review*, *133*(5), 1076–1097. Re-
334 trieved from [https://journals.ametsoc.org/view/journals/mwre/133/
335 5/mwr2905.1.xml](https://journals.ametsoc.org/view/journals/mwre/133/5/mwr2905.1.xml) doi: 10.1175/MWR2905.1
- 336 Cavaleri, L., Fox-Kemper, B., & Hemer, M. (2012). Wind waves in the coupled cli-
337 mate system. *Bulletin of the American Meteorological Society*. doi: 10.1175/
338 BAMS-D-11-00170.1
- 339 Crosby, S. C., Cornuelle, B. D., O’Reilly, W. C., & Guza, R. T. (2017, 8). Assim-
340 ilating Global Wave Model Predictions and Deep-Water Wave Observations in
341 Nearshore Swell Predictions. *Journal of Atmospheric and Oceanic Technol-
342 ogy*, *34*(8), 1823–1836. Retrieved from [https://journals.ametsoc.org/
343 view/journals/atot/34/8/jtech-d-17-0003.1.xml](https://journals.ametsoc.org/view/journals/atot/34/8/jtech-d-17-0003.1.xml) doi: 10.1175/
344 JTECH-D-17-0003.1
- 345 Hasselmann, S., Lionello, P., & Hasselmann, K. (1997). An optimal interpolation
346 scheme for the assimilation of spectral wave data. *Journal of Geophysical Re-
347 search C: Oceans*, *102*(C7), 15823–15836. doi: 10.1029/96JC03453
- 348 Houghton, I. A., Smit, P. B., Clark, D., Dunning, C., Fisher, A., Nidziedo, N. J., ...
349 Janssen, T. T. (2021, 5). Performance Statistics of a Real-Time Pacific Ocean
350 Weather Sensor Network. *Journal of Atmospheric and Oceanic Technology*,
351 *38*(5), 1047–1058. Retrieved from [https://journals.ametsoc.org/view/
352 journals/atot/aop/JTECH-D-20-0187.1/JTECH-D-20-0187.1.xml](https://journals.ametsoc.org/view/journals/atot/aop/JTECH-D-20-0187.1/JTECH-D-20-0187.1.xml) doi:
353 10.1175/JTECH-D-20-0187.1
- 354 Kalnay, E. (2002, 11). Atmospheric Modeling, Data Assimilation and Predictabil-
355 ity. *Atmospheric Modeling, Data Assimilation and Predictability*. doi: 10.1017/
356 CBO9780511802270
- 357 Kuik, A. J., van Vledder, G. P., & Holthuijsen, L. H. (1988). A Method for the Rou-
358 tine Analysis of Pitch-and-Roll Buoy Wave Data. *Journal of Physical Oceanog-
359 raphy*. doi: 10.1175/1520-0485(1988)018<1020:amftra>2.0.co;2
- 360 Lionello, P., Gunther, H., & Janssen, P. A. (1992). Assimilation of altimeter data in
361 a global third-generation wave model. *Journal of Geophysical Research*. doi: 10
362 .1029/92jc01055
- 363 Lygre, A., & Krogstad, H. E. (1986). Maximum Entropy Estimation of the Direc-
364 tional Distribution in Ocean Wave Spectra. *Journal of Physical Oceanography*,
365 *16*(12), 2052–2060. Retrieved from [https://journals.ametsoc.org/view/
366 journals/phoc/16/12/1520-0485_1986_016_2052_meeotd_2_0_co_2.xml](https://journals.ametsoc.org/view/journals/phoc/16/12/1520-0485_1986_016_2052_meeotd_2_0_co_2.xml) doi:
367 10.1175/1520-0485(1986)016<2052:MEEOTD>2.0.CO;2
- 368 Portilla, J., Ocampo-Torres, F. J., & Monbaliu, J. (2009, 1). Spectral Par-
369 titioning and Identification of Wind Sea and Swell. *Journal of Atmo-
370 spheric and Oceanic Technology*, *26*(1), 107–122. Retrieved from [https://
371 journals.ametsoc.org/view/journals/atot/26/1/2008jtecho609.1.xml](https://journals.ametsoc.org/view/journals/atot/26/1/2008jtecho609.1.xml)
372 doi: 10.1175/2008JTECHO609.1
- 373 Portilla-Yandún, J., & Cavaleri, L. (2016, 1). On the specification of background
374 errors for wave data assimilation systems. *Journal of Geophysical Research:
375 Oceans*, *121*(1), 209–223. doi: 10.1002/2015JC011309
- 376 Raghukumar, K., Chang, G., Spada, F., Jones, C., Janssen, T., & Gans, A. (2019).
377 Performance characteristics of ”spotter,” a newly developed real-time wave
378 measurement buoy. *Journal of Atmospheric and Oceanic Technology*, *36*(6),
379 1127–1141. doi: 10.1175/JTECH-D-18-0151.1
- 380 Smit, P. B., Houghton, I. A., Jordanova, K., Portwood, T., Shapiro, E., Clark,
381 D., ... Janssen, T. T. (2021, 3). Assimilation of significant wave height
382 from distributed ocean wave sensors. *Ocean Modelling*, *159*, 101738. doi:
383 10.1016/J.OCEMOD.2020.101738
- 384 Thomas, J. P. (1988, 4). Retrieval of energy spectra from measured data for as-

- 385 simulation into a wave model. *Quarterly Journal of the Royal Meteorological*
 386 *Society*, 114(481), 781–800. Retrieved from <https://rmets.onlinelibrary>
 387 [.wiley.com/doi/full/10.1002/qj.49711448112](https://rmets.onlinelibrary.wiley.com/doi/full/10.1002/qj.49711448112)
 388 <https://rmets.onlinelibrary.wiley.com/doi/abs/10.1002/qj.49711448112>
 389 [doi: 10.1002/qj.49711448112](https://rmets.onlinelibrary.wiley.com/doi/10.1002/qj.49711448112)
 390 [doi: 10.1002/QJ.49711448112](https://doi.org/10.1002/QJ.49711448112)
- 391 Tolman, H., Abdolali, A., Accensi, M., Alves, J.-H., Ardhuin, F., Babanin, A.,
 392 ... Liang, Z. (2019). *User manual and system documentation of WAVE-*
 393 *WATCH III (R) version 6.07* (Tech. Rep.). Retrieved from [https://](https://www.researchgate.net/publication/336069899_User_manual_and_system_documentation_of_WAVEWATCH_III_R_version_607)
 394 [www.researchgate.net/publication/336069899_User_manual_and_system](https://www.researchgate.net/publication/336069899_User_manual_and_system_documentation_of_WAVEWATCH_III_R_version_607)
 395 [_documentation_of_WAVEWATCH_III_R_version_607](https://www.researchgate.net/publication/336069899_User_manual_and_system_documentation_of_WAVEWATCH_III_R_version_607)
- 396 Voermans, J. J., Smit, P. B., Janssen, T. T., & Babanin, A. V. (2020). Estimatin
 397 g Wind Speed and Direction Using Wave Spectra. *Journal of Geophysical*
 398 *Research: Oceans*. doi: 10.1029/2019JC015717
- 399 Voorrips, A. C., Makin, V. K., & Hasselmann, S. (1997). Assimilation of wave spec
 400 tra from pitch-and-roll buoys in a North Sea wave model. *Journal of Geophysic*
 401 *al Research C: Oceans*, 102(C3), 5829–5849. doi: 10.1029/96JC03242